Room-temperature continuous-wave operation of membrane distributed-reflector laser

2015 Appl. Phys. Express 8 112701

(http://iopscience.iop.org/1882-0786/8/11/112701)

Applied Physics Express **8**, 112701 (2015)
http://dx.doi.org/**10.7567/APEX.8.112701**

Room-temperature continuous-wave operation of membrane distributed-reflector laser

Takuo Hiratani[1]*, Daisuke Inoue[1], Takahiro Tomiyasu[1], Yuki Atsuji[1], Kai Fukuda[1], Tomohiro Amemiya[2], Nobuhiko Nishiyama[1], and Shigehisa Arai[1,2]

[1]*Department of Electrical and Electronic Engineering, Tokyo Institute of Technology, Meguro, Tokyo 152-8552, Japan*
[2]*Quantum Nanoelectronics Research Center, Tokyo Institute of Technology, Meguro, Tokyo 152-8552, Japan*
E-mail: hiratani.t.aa@m.titech.ac.jp

Received September 10, 2015; accepted September 25, 2015; published online October 20, 2015

In this paper, we report on the first ever demonstration of a continuous-wave operation of an injection-type membrane distributed-reflector (DR) laser at room temperature. A threshold current of 250 μA was obtained with a stripe width of 0.7 μm, a DFB region length of 30 μm, and a DBR region length of 90 μm. An external differential quantum efficiency of 11% with a light output ratio between the front and the rear of 6.7 was obtained at the front waveguide.

Recent progress in the scaling of large-scale integrated circuits (LSIs)[1] has resulted in a high data processing speed. However, problems such as signal delay and significant power dissipation that occur in long electrical wires to functional blocks exist.[2,3] These will become critical problems for LSI in the near future. On-chip optical interconnection has been proposed as an attractive candidate to overcome these problems, with low-power and high-speed data transmission expected.[4–6] Light sources with ultralow-power consumption have been presented. They include ultrasmall cavity lasers such as microdisk lasers,[7,8] vertical cavity surface-emitting lasers (VCSELs),[9,10] and photonic crystal lasers.[11–13] The required energy for these light sources is estimated to be less than 100 fJ/bit.[14] Photonic crystal lasers are attractive candidates for in-plane integration, with an ultralow energy consumption of 4.4 fJ/bit using an avalanche photodiode (APD) that was previously reported.[15] The sensitivity of an APD is 10 times higher than that of normal photodiodes; however, the applied bias voltage is also higher by a factor of 10 or more, and such a high bias voltage seems not to be consistent with future LSIs where the source voltage tends to decrease to 1.0 V or less.

We estimated the required light output power of more than 0.16 mW when the minimum receivable power of a pin-PD was assumed to be −13 dBm (50 μW) for a bit error rate (BER) of 10^{-9} at a signal speed of 10 Gbps and the link loss was assumed to be 5 dB. A membrane DFB laser was proposed and demonstrated to satisfy these requirements.[16,17] The membrane structure is advantageous for ultralow-threshold operation because it has a strong optical confinement owing to a high-index-contrast waveguide. In this structure, the lateral current injection (LCI)[18] is adopted because the vertical injection used in conventional laser diodes cannot be utilized. A DFB laser on a SiO_2/Si substrate with a threshold current of 0.9 mA and an energy cost of 171 fJ/bit for a 25.8 Gbps NRZ signal has recently been reported.[19] Furthermore, our group previously demonstrated a membrane DFB laser with a butt-jointed built-in (BJB) structure.[20] In that laser, we obtained a threshold current of 230 μA and an external differential quantum efficiency from the front waveguide side of 5%.

In this paper, we report on the first ever realization of LCI-membrane distributed-reflector (DR) lasers. A threshold current of 250 μA and an external differential quantum efficiency of 11% were obtained with an asymmetric light output ratio of 6.7 between the front and the rear. Furthermore, the calculation indicated that a higher light output can be expected with a reduction in waveguide loss in the passive section.

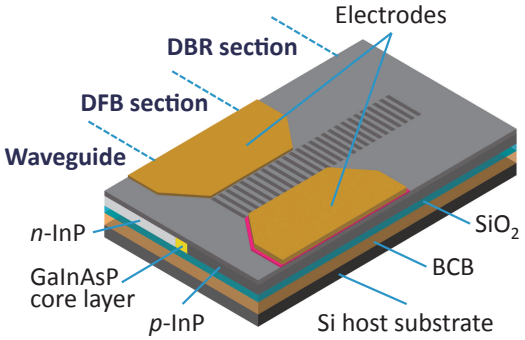

Fig. 1. Schematic structure of LCI-membrane DR laser.

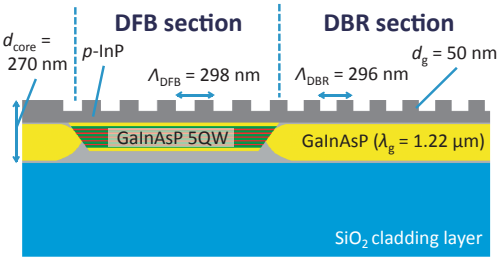

Fig. 2. Cross-sectional view of the LCI-membrane DR laser.

Figure 1 shows a schematic of the LCI-membrane DR laser. It consists of an active DFB section and a passive DBR section. The passive waveguide was formed by the BJB regrowth process, and the DFB and DBR structures were realized by a surface grating.[21] The DBR at one side of the DFB structure facilitates the concentration of the light output at the opposite side of the DFB structure. Figure 2 shows the cross section along the cavity direction of the LCI-membrane DR laser where the surface grating depth (d_g) of 50 nm was found in both the DFB and DBR sections for a simple etching process. We adopted a period of 298 nm for the DFB section (Λ_{DFB}) and that of 296 nm for the DBR section (Λ_{DBR}) in order to match the lasing wavelength to the Bragg wavelength of the DBR section. A small reduction in period in the DBR section of the membrane laser is needed because the membrane DFB laser with a surface grating typically operates at the short-wavelength side of the stop band

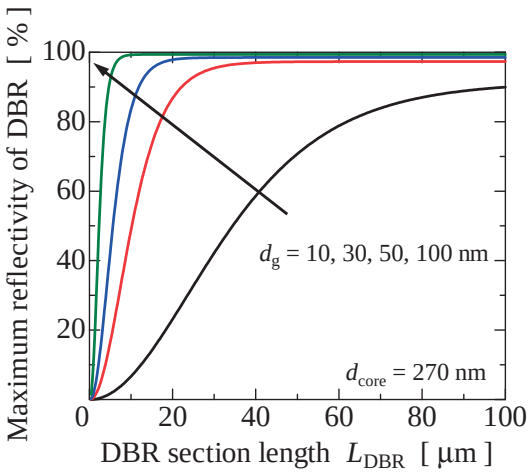

Fig. 3. Maximum reflectivity dependence on DBR section length for various grating depths (d_g) for $d_{core} = 270$ nm as shown in Fig. 2.

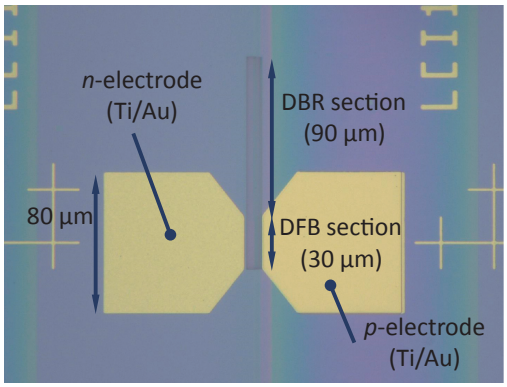

Fig. 4. Photomicrograph of fabricated device.

because of its strong optical confinement to the low-index region of the grating.[20)]

Furthermore, the reflectivity tolerance for the grating depth was calculated to determine the length of the DBR section. Figure 3 shows the maximum reflectivity of the DBR at the Bragg wavelength as a function of the DBR section length for various grating depths (d_g), where the core thickness (d_{core}) was fixed at 270 nm. Here, the waveguide loss of 12 cm^{-1} in the passive section was assumed by taking into account the transverse mode profile and p-InP loss from intervalence band absorption.[22)] It is shown that the structure with a high index-coupling coefficient enables a shorter DBR section length. The grating depth of 100 nm corresponds to the index-coupling coefficient of 4000 cm^{-1}. The DBR section length of 90 μm was used for the fabrication to obtain a reflectivity higher than 95% for various grating depths larger than 30 nm.

We used the same initial wafer with a core thickness of 270 nm including five QWs, and the process is the same as that used in our previous work[20)] to fabricate the LCI-membrane DR laser. The fabrication includes a three-step regrowth for the formation of a waveguide and a pin structure, BCB bonding to the Si host substrate, evaporation of electrodes, and formation of a surface grating. Figure 4 shows a photomicrograph of the fabricated device. We can confirm the formation of the DFB and DBR sections from the image.

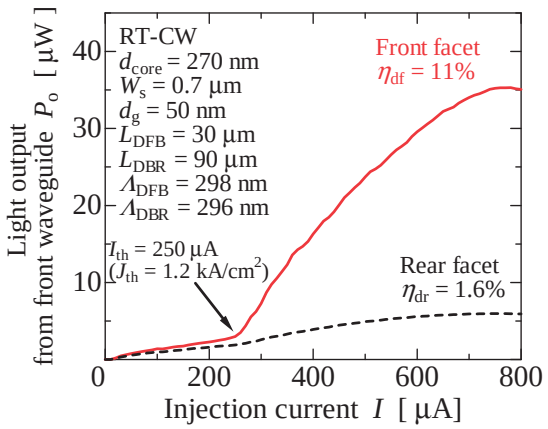

Fig. 5. Light output–injection current characteristics of LCI-membrane DR laser.

The static characteristics of the fabricated LCI-membrane DR laser with a core thickness (d_{core}) of 270 nm, a stripe width (W_s) of 0.7 μm, a DFB section length (L_{DFB}) of 30 μm, and a DBR section length (L_{DBR}) of 90 μm were measured. The device was formed by cleavage and had an approximately 200-μm-long waveguide at the front side and a 100-μm-long waveguide at the rear side.

Figure 5 shows the light output characteristics of the LCI-membrane DR laser outlined above. A threshold current (I_{th}) of 250 μA [corresponding to a threshold current density (J_{th}) of 1.2 kA/cm^2], an external differential quantum efficiency at the front side (η_{df}) of 11% (indicated by the solid line), and that at the rear side (η_{dr}) of 1.6% (indicated by the dashed line) were obtained under room-temperature continuous-wave (RT-CW) operation. Furthermore, the threshold voltage (V_{th}) of 3.5 V and the device resistance (R_s) of approximately 6400 Ω were obtained. In order to realize low-power-consumption operation as well as high-speed modulation, reductions in these values are required.

Although the coupling strength of the DBR section was estimated to be quite large ($\kappa L = 11.7$ for $\kappa = 1300$ cm^{-1} and $L = 90$ μm), η_{dr} of 1.6% was quite large compared with the expected value. This is considered to be caused by a slight deviation (approximately 14 nm) of the Bragg wavelength of the DBR section from the lasing wavelength, which is mostly defined by the DFB section. A light output ratio between the front and the rear of 6.7 and a maximum light output power of 35.3 μW at the bias current of 780 μA were realized. These results show that approximately twice the light output was obtained with virtually the same threshold current compared with that of the membrane DFB laser in a previous work[20)] by introducing the DR structure.

The lasing spectrum of the device at a bias current of $2I_{th}$ (= 500 μA) is shown in Fig. 6, where a single-mode operation at 1545 nm with a side-mode suppression ratio (SMSR) of 22 dB and a stopband width of 29 nm, from which the index-coupling coefficient (κ_i) of the grating was estimated to be 1300 cm^{-1}, were observed. A higher SMSR can be expected by adjusting the Bragg wavelength of the DBR section relative to the gain peak wavelength.

In order to discuss these results quantitatively, theoretical analysis was carried out. Figure 7 shows the DFB section length dependences of (a) threshold current (I_{th}) and (b) external differential quantum efficiency from the front side

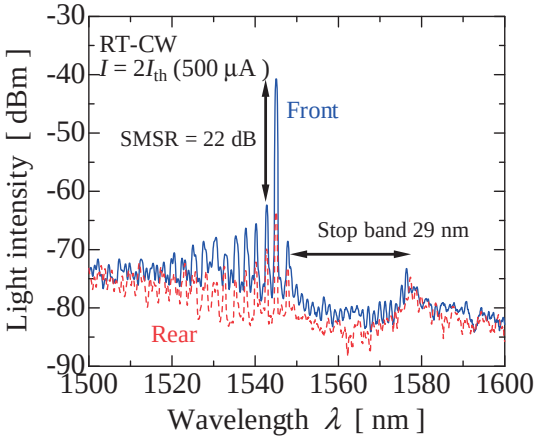

Fig. 6. Lasing spectrum of LCI-membrane DR laser.

(η_{df}) of three types of membrane laser, namely, uniform DFB laser, uniform DR laser, and DR laser with a $\lambda/4$-shift region, calculated by the transfer-matrix method (TMM).[23] In the calculation, a core thickness (d_{core}) of 270 nm, a stripe width (W_s) of 0.7 μm, a surface grating depth of 50 nm, and an internal quantum efficiency (η_i) of 0.75[24] were used. The $\lambda/4$-shift was set at a position of 0.7 L_{DFB} from the front side of the DFB section in order to obtain a high η_{df} while maintaining a low threshold current. Although the threshold current of the device shown in Fig. 5 was in agreement with the theoretically calculated value [Fig. 7(a)], η_{df} was only 1/6 of the theoretical value, as shown in Fig. 7(b). The reason for the low η_{df} is considered to be the relatively high waveguide loss in the passive section and a slight deviation of the Bragg wavelength of the DBR section from that of the DFB section. Because the I_{th} of the uniform DR laser was found to be much lower than that of the uniform DFB laser, as shown in Fig. 7(a), the optical coupling loss between the active and passive sections was considered to be negligibly small; however, the optical loss in the passive waveguide section may be a possible reason for this difference. In fact, the passive waveguide region was fabricated by a two-step (n-InP and p-InP) regrowth, and the scattering may have occurred at the regrown boundaries between the GaInAsP core and the p-InP or n-InP cladding layers. Moreover, p-InP has a relatively large absorption coefficient (20 cm^{-1} for a doping concentration of 1×10^{18} cm^{-3} [22]). The waveguide loss in the passive section is estimated to be 12 cm^{-1} by considering the heavily doped p-InP cladding layer (4×10^{18} cm^{-3}). Therefore, it is very important to clarify the optical loss in the passive waveguide section in order to realize a high η_{df} as well as a high output power in LCI-membrane DR lasers. In addition to the waveguide loss in the passive waveguide section, a slight deviation of the Bragg wavelength of the DBR section from the lasing wavelength defined by the DFB section might also be responsible for the poor differential quantum efficiency from the front side. This is caused by the design of the period of DBR. If these problems are solved, an η_{df} of 67% can be expected for a uniform DR laser with a DFB section length of 30 μm. Furthermore, as shown in Fig. 7, a lower threshold current of 66 μA as well as an η_{df} of 30% can be obtained for a $\lambda/4$-phase-shifted DR laser with a DFB section length of 27 μm. These results show that the LCI-membrane DR laser

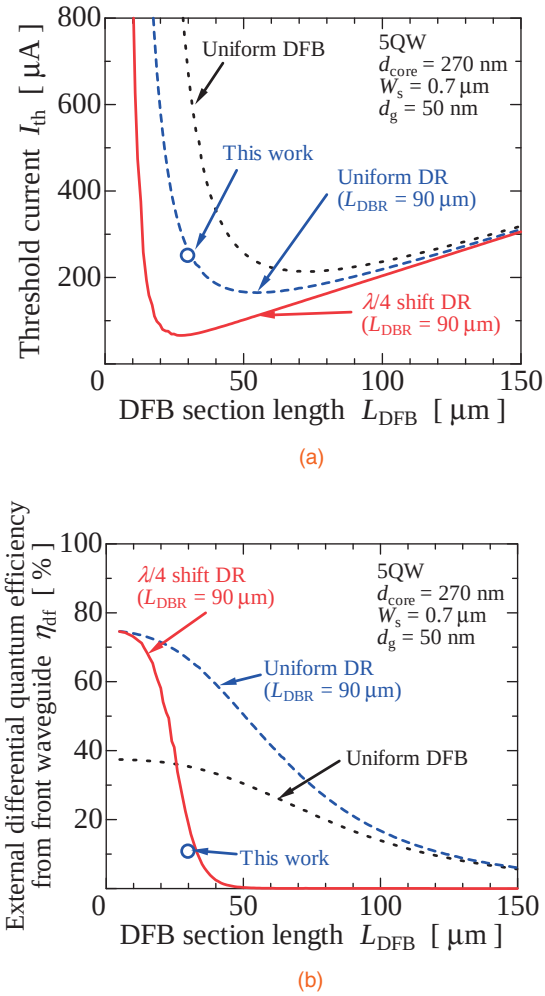

Fig. 7. Calculated DFB section length dependences of (a) threshold current and (b) external differential quantum efficiency for various types of membrane laser.

is an attractive candidate light source with ultralow-power-consumption operation.

In conclusion, a membrane DR laser, aimed at providing the light source for on-chip optical interconnection, was realized and its RT-CW operation was demonstrated for the first time. A threshold current of 250 μA, which showed good agreement with the theoretically calculated value, was obtained for DFB and DBR section lengths of 30 and 90 μm. On the other hand, although an external differential quantum efficiency from the front side (η_{df}) of 11%, which was 6.7 times higher than that from the rear side, also indicated an efficient reflection of the passive DBR section, it was very low compared with the theoretically calculated value. Comparisons between the experimental and theoretical results indicate that the optical loss in the passive waveguide section and the deviation of the Bragg wavelength of the DBR section from the lasing wavelength are responsible for the poor external differential quantum efficiency, whereas the coupling loss between the active and passive sections can be regarded as negligibly small.

Acknowledgments The authors would like to thank Professors S. Akiba, T. Mizumoto, M. Asada, and Y. Miyamoto, and Associate Professor M. Watanabe of the Tokyo Institute of Technology for their fruitful discussions. This work was supported by JSPS KAKENHI Grant Numbers 24246061, 25709026, 25420321, 15H05763, 15J04654, and 15J11776.

1) R. H. Dennard, IEEE Solid-State Circuits Mag. **7** [2], 29 (2015).
2) P. Kapur, J. P. McVittie, and K. C. Saraswat, IEEE Trans. Electron Devices **49**, 590 (2002).
3) P. Kapur, G. Chandra, J. P. McVittie, and K. C. Saraswat, IEEE Trans. Electron Devices **49**, 598 (2002).
4) D. A. B. Miller, Proc. IEEE **88**, 728 (2000).
5) G. Chen, H. Chen, M. Haurylau, N. A. Nelson, D. H. Albonesi, P. M. Fauchet, and E. G. Friedman, Integration–VLSI J. **40**, 434 (2007).
6) K. Ohashi, K. Nishi, T. Shimizu, M. Nakada, J. Fujikata, J. Ushida, S. Torii, K. Nose, M. Mizuno, H. Yukawa, M. Kinoshita, N. Suzuki, A. Gomyo, T. Ishi, D. Okamoto, K. Furue, T. Ueno, T. Tsuchizawa, T. Watanabe, K. Yamada, S. Itabashi, and J. Akedo, Proc. IEEE **97**, 1186 (2009).
7) M. Fujita, R. Ushigome, and T. Baba, Electron. Lett. **36**, 790 (2000).
8) J. Van Campenhout, P. Rojo-Romeo, P. Regreny, C. Seassal, D. Van Thourhout, S. Verstuyft, L. Di Cioccio, J.-M. Fedeli, C. Lagahe, and R. Baets, Opt. Express **15**, 6744 (2007).
9) P. Moser, W. Hofmann, P. Wolf, J. A. Lott, G. Larisch, A. Payusov, N. N. Ledentsov, and D. Bimberg, Appl. Phys. Lett. **98**, 231106 (2011).
10) A. Kasukawa, IEEE Photonics J. **4**, 642 (2012).
11) S. Matsuo, A. Shinya, T. Kakitsuka, K. Nozaki, T. Segawa, T. Sato, Y. Kawaguchi, and M. Notomi, Nat. Photonics **4**, 648 (2010).
12) B. Ellis, M. A. Mayer, G. Shambat, T. Sarmiento, J. Harris, E. E. Haller, and J. Vučković, Nat. Photonics **5**, 297 (2011).
13) S. Matsuo, T. Sato, K. Takeda, A. Shinya, K. Nozaki, H. Taniyama, M. Notomi, K. Hasebe, and T. Kakitsuka, IEEE J. Sel. Top. Quantum Electron. **19**, 4900311 (2013).
14) D. A. B. Miller, Proc. IEEE **97**, 1166 (2009).
15) K. Takeda, T. Sato, A. Shinya, K. Nozaki, W. Kobayashi, H. Taniyama, M. Notomi, K. Hasebe, T. Kakitsuka, and S. Matsuo, Nat. Photonics **7**, 569 (2013).
16) T. Okamoto, N. Nunoya, Y. Onoda, T. Yamazaki, S. Tamura, and S. Arai, IEEE J. Sel. Top. Quantum Electron. **9**, 1361 (2003).
17) S. Arai, N. Nishiyama, T. Maruyama, and T. Okumura, IEEE J. Sel. Top. Quantum Electron. **17**, 1381 (2011).
18) K. Oe, Y. Noguchi, and C. Caneau, IEEE Photonics Technol. Lett. **6**, 479 (1994).
19) S. Matsuo, T. Fujii, K. Hasebe, K. Takeda, T. Sato, and T. Kakitsuka, J. Lightwave Technol. **33**, 1217 (2015).
20) D. Inoue, J. Lee, T. Hiratani, Y. Atsuji, T. Amemiya, N. Nishiyama, and S. Arai, Opt. Express **23**, 7771 (2015).
21) T. Shindo, T. Okumura, H. Ito, T. Koguchi, D. Takahashi, Y. Atsumi, J. Kang, R. Osabe, T. Amemiya, N. Nishiyama, and S. Arai, Opt. Express **19**, 1884 (2011).
22) H. C. Casey, Jr. and P. L. Carter, Appl. Phys. Lett. **44**, 82 (1984).
23) G. Bjork and O. Nilsson, J. Lightwave Technol. **5**, 140 (1987).
24) D. Inoue, J. Lee, K. Doi, T. Hiratani, Y. Atsuji, T. Amemiya, N. Nishiyama, and S. Arai, Appl. Phys. Express **7**, 072701 (2014).